

High-Performance Near-IR Photodetector Using Low-Bandgap MA_{0.5}FA_{0.5}Pb_{0.5}Sn_{0.5}I₃ Perovskite

Xiaobao Xu, Chu-Chen Chueh, Peifeng Jing, Zhibin Yang, Xueliang Shi, Ting Zhao, Lih Y. Lin, and Alex K.-Y. Jen*

Photodetectors with ultrafast response are explored using inorganic/organic hybrid perovskites. High responsivity and fast optoelectronic response are achieved due to the exceptional semiconducting properties of perovskite materials. However, most of the perovskite-based photodetectors exploited to date are centered on Pb-based perovskites, which only afford spectral response across the visible spectrum. This study demonstrates a high-performance near-IR (NIR) photodetector using a stable low-bandgap Sn-containing perovskite, (CH₃NH₃)_{0.5}(NH₂CHNH₂)_{0.5}Pb_{0.5}Sn_{0.5}I₃ (MA_{0.5}FA_{0.5}Pb_{0.5}Sn_{0.5}I₃), which is processed with an antioxidant additive, ascorbic acid (AA). The addition of AA effectively strengthens the stability of Sn-containing perovskite against oxygen, thereby significantly inhibiting the leakage current. Consequently, the derived photodetector shows high responsivity with a detectivity of over 10¹² Jones ranging from 800 to 970 nm. Such low-cost, solution processable NIR photodetectors with high performance show promising potential for future optoelectronic applications.

1. Introduction

Photodetectors that transduce optical signals into electric signal have served as important function components in many optoelectronic applications, such as fluorescence microscopy, spectroscopy, clinical chemistry, imaging, chemical/environmental/elemental analysis, and the scientific research.^[1–4] In general, photodetectors can be defined into two types, the broad-band type and the narrow-band type, based on the spectral response bandwidth of the photoactive materials. The key figure-of-merit

(FOM) parameters of a photodetector which determine their usefulness are responsivity (R), detectivity (D^*), noise equivalent power (NEP), linear dynamic range (LDR), and response speed. To date, myriads of efforts have been devoted to improve the FOM of photodetectors.

In the past decades, various solution-processed photodetectors have been developed by using low-cost organic semiconductors^[5–7] and nanomaterials.^[8,9] Many of them have been demonstrated with a laudable response rate and detectivity rivaling the performance of traditional inorganic semiconductors like silicon and InGaAs^[10] that are fabricated by sophisticated and quite costly vacuum-deposition procedures. Recently, the hybrid perovskite-based photodetectors have attracted significant research attention due to the exceptional semiconducting properties of

organic/inorganic hybrid perovskites (ABX₃, where A is a monovalent cation [CH₃NH₃⁺ (MA), NH₂CHNH₂⁺ (FA), or Cs⁺], B is a divalent metal cation (Pb²⁺ or Sn²⁺), and X is a halide anion (Cl⁻, Br⁻, or I⁻)),^[11–13] including intense light-harvesting capability and excellent charge carrier mobility.^[14–17] In addition, the facile solution processability of perovskites combining their diversity in structure modifications affords promising merits for practical applications.^[18,19]

It is worth mentioning that the optical bandgap (E_g) of such materials can be manipulated by engineering their compositions.^[20,21] The pristine Pb-based perovskites (APbX₃) generally possess an absorption edge located in the visible region while the Sn-based family (ASnX₃) shows an extended absorption edge to near-IR (NIR) wavelengths. Therefore, by increasing the Sn ratio in perovskite compositions, one can gradually expand the photoresponse of perovskite materials to the NIR region. Taking MAPb_{1-x}Sn_xI₃ as an example, the resulting optical E_g can be tuned from 1.55 to 1.17 eV by gradually increasing the Sn content in the composition.^[22–26] This feature provides great potential for this class of materials to be used for photodetectors, which requires fast, sensitive, low-cost, and spectrally tunable materials.

Numerous perovskite photodetectors have been shown to possess high responsivity, excellent detectivity, large photo-to-dark current ratio, and fast response.^[27,28] However, most of them are designed to detect visible light,^[27,28] with some for X-ray and gamma-ray,^[29] while efficient perovskite photodetectors for the NIR region are still lacking due to easy oxidation

Dr. X. Xu, Dr. C.-C. Chueh, Dr. Z. Yang, Dr. X. Shi, Dr. T. Zhao,
Prof. A. K.-Y. Jen
Department of Materials Science and Engineering
University of Washington
Seattle, WA 98195-2120, USA
E-mail: ajen@uw.edu

Dr. C.-C. Chueh
Department of Chemical Engineering
National Taiwan University

Dr. P. Jing, Prof. L. Y. Lin
Department of Electrical Engineering
University of Washington
Seattle, WA 98195-2120, USA

Prof. A. K.-Y. Jen
Department of Biology and Chemistry
City University of Hong Kong
Kowloon, Hong Kong

DOI: 10.1002/adfm.201701053

and fast crystallization of Sn-containing perovskites preventing the fabrication of high-quality films.^[26]

In this study, we report, for the first time, a perovskite photodetector with a high-performance NIR detector by using a stable low E_g Sn-containing binary perovskite, $\text{MA}_{0.5}\text{FA}_{0.5}\text{Pb}_{0.5}\text{Sn}_{0.5}\text{I}_3$, which is processed with an antioxidant additive, ascorbic acid (AA).^[30] The AA additive with the laudable antioxidant property can not only retard the formation of Sn vacancy caused by the Sn oxidation but also facilitate the film formation by modulating the perovskite crystallization kinetics. As a result, the derived photodetector possesses an inhibited leakage current and an enhanced signal-to-noise ratio, achieving a high responsivity of over 0.1 A W^{-1} with a detectivity of over 10^{12} Jones ranging from 800 to $\approx 1000 \text{ nm}$.

2. Results and Discussion

As mentioned earlier, the Sn-containing perovskites generally degrade rapidly due to their propensity to oxidation, which engenders the poor reproducibility and device performance.^[31] To address this issue, we have recently introduced AA, which is a decent antioxidant as additive to assist the processing of Sn-containing perovskite.^[30,32] It was revealed that the AA additive can not only retard the Sn^{+2} oxidation but also promote the film formation since the counter anion of AA can serve as a Lewis base to modulate the crystallization kinetics and to passivate the associated Sn-derived defects. As a result, the performance and stability of Sn-containing perovskite solar cells were significantly improved,^[30] which outperform those using conventional SnF_2 as a processing additive.^[33,34]

Figure 1a presents the top view scanning electron microscopy (SEM) image of the fabricated $\text{MA}_{0.5}\text{FA}_{0.5}\text{Pb}_{0.5}\text{Sn}_{0.5}\text{I}_3$ film with the AA additive, wherein a uniform and compact morphology can be clearly observed. The method for depositing the perovskite films adopted the solvent-washing technique^[25] and the details are described in the “Experimental Section.” The corresponding X-ray diffraction (XRD) profile of $\text{MA}_{0.5}\text{FA}_{0.5}\text{Pb}_{0.5}\text{Sn}_{0.5}\text{I}_3$ film with/without the AA additive is shown in **Figure 1b**, where the characteristic peaks well indexed the formation of perovskite, and their sharp feature indicates high crystallinity of the prepared film. All these results validate the high quality of $\text{MA}_{0.5}\text{FA}_{0.5}\text{Pb}_{0.5}\text{Sn}_{0.5}\text{I}_3$ film derived from the AA additive, which endows its outstanding concomitant optoelectronic properties for device applications.

To confirm the enhanced antioxidative property enabled by AA additive, we have compared the electrochemical impedance spectroscopy (EIS) spectra of the $\text{MA}_{0.5}\text{FA}_{0.5}\text{Pb}_{0.5}\text{Sn}_{0.5}\text{I}_3$ films derived from SnF_2 and AA additives in a dummy cell configuration measured at 0 V bias in dark. As shown in **Figure S1** (Supporting Information), the resistance of the SnF_2 -derived film

decreased significantly after storing in air for 3 h while the AA-derived film maintained at the similar level. The enhanced conductivity of the SnF_2 -derived film can be traced to its increased carrier density due to Sn^{2+} oxidation.^[20] This result clearly reveals the better antioxidative property of AA additive over SnF_2 , for which it acts as an effective oxidation scavenger due to its C=C double bond.^[30,35]

The perovskite photodetector using $\text{MA}_{0.5}\text{FA}_{0.5}\text{Pb}_{0.5}\text{Sn}_{0.5}\text{I}_3$ is then fabricated in the configuration of ITO(indium tin oxide)/PEDOT(poly(3,4-ethylenedioxythiophene)):PSS(poly(styrenesulfonate))/ $\text{MA}_{0.5}\text{FA}_{0.5}\text{Pb}_{0.5}\text{Sn}_{0.5}\text{I}_3$ /PC₆₁BM(phenyl-C61-butyric acid methyl ester)/bis-C₆₀/Ag. The cross-sectional SEM image shown in **Figure 1c** clearly illustrates its stratified architecture, where the thicknesses of the PEDOT:PSS, PCBM, and perovskite layer are ≈ 30 , 50, and 300–350 nm, respectively. The normalized absorption of the $\text{MA}_{0.5}\text{FA}_{0.5}\text{Pb}_{0.5}\text{Sn}_{0.5}\text{I}_3$ film along with the external quantum efficiency (EQE) of its derived photodiode is illustrated in **Figure 1d**. As shown, the $\text{MA}_{0.5}\text{FA}_{0.5}\text{Pb}_{0.5}\text{Sn}_{0.5}\text{I}_3$ film possesses an estimated E_g of 1.24 eV, which results in a broad photoresponse between 350 and 1000 nm of the derived device. The photoluminescence (PL) spectrum of our $\text{MA}_{0.5}\text{FA}_{0.5}\text{Pb}_{0.5}\text{Sn}_{0.5}\text{I}_3$ film is also presented in **Figure S2** (Supporting Information). Similar to our previous study,^[26] the bandgap evaluated from PL is larger than the value extracted from the corresponding UV–vis absorption spectrum. This clearly verifies its potential application for NIR photodetector or for all perovskite tandem photovoltaics.^[36] To make it different from the traditional MAPbI_3 , we will focus on the optoelectronic property of this photodiode for wavelength ranging from 800 to 1000 nm.

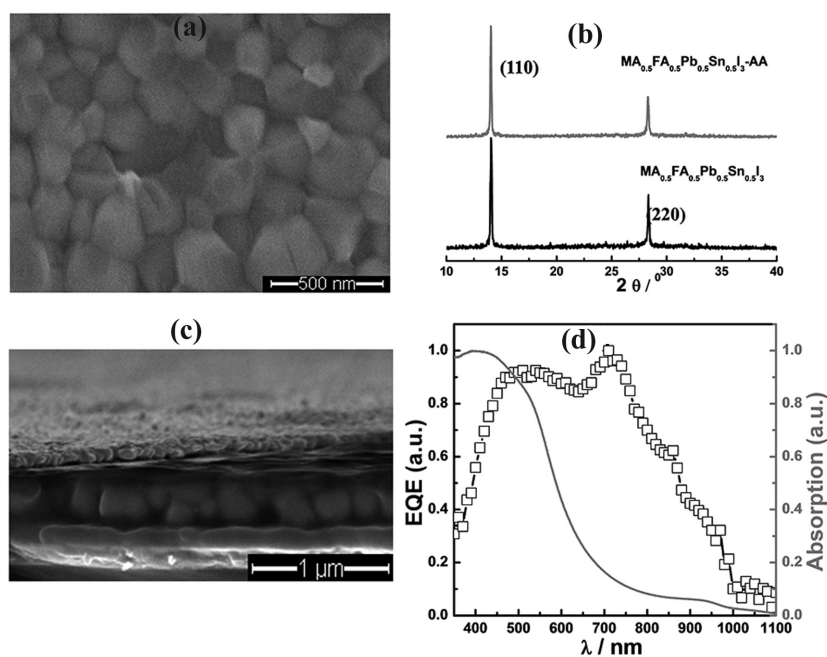


Figure 1. a) Top-view SEM image of $\text{MA}_{0.5}\text{FA}_{0.5}\text{Pb}_{0.5}\text{Sn}_{0.5}\text{I}_3$ film with AA additive. b) The corresponding XRD profile of the $\text{MA}_{0.5}\text{FA}_{0.5}\text{Pb}_{0.5}\text{Sn}_{0.5}\text{I}_3$ film. c) The cross-sectional SEM image of the photodiode with a configuration of ITO/PEDOT:PSS/perovskite/PC₆₁BM/bis-C₆₀/Ag. d) The normalized UV–vis absorption spectrum of $\text{MA}_{0.5}\text{FA}_{0.5}\text{Pb}_{0.5}\text{Sn}_{0.5}\text{I}_3$ film and the EQE of its derived photodetector.

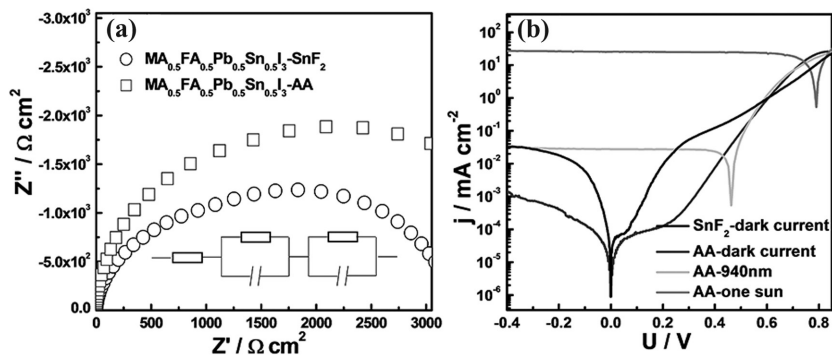


Figure 2. a) The Nyquist plots of the studied photodetectors derived from different additives measured in dark without biasing (inserted is lumped RC-circuit). b) J - V curves of the studied photodetectors measured in dark and under illumination.

The corresponding photocurrent density–voltage (J - V) characteristics under AM 1.5 (100 mW cm^{-2}) and the statistic of the fabricated photodiodes are presented in Figure S3 (Supporting Information). As can be seen, the AA-derived photodiode showed an enhanced photovoltage, which indicates lower defect recombination of photogenerated charges.^[37] Note that the hysteresis still exists in J - V curves with different scan direction. The EIS measurements of the photodiodes were also conducted and the corresponding Nyquist plots were shown in Figure 2a. By fitting the measured curves with a lumped RC-circuit (resistance-capacitance circuit),^[38] the interfacial charge recombination resistance of the AA-derived device was estimated to be $3373 \text{ } \Omega \text{ cm}^2$, which exceeds the value ($2285 \text{ } \Omega \text{ cm}^2$) of the SnF_2 -derived device. Under illumination (as shown in Figure S4 of the Supporting Information), the interfacial recombination resistance in the device with AA is almost two times larger than that in the device with SnF_2 . This clearly manifests the reduced leakage current in the AA-derived device.^[39] Note that the high leakage current of a photodiode has been cited as a main factor that ruins the device performance.^[40]

Figure 2b shows the J - V characteristics of the SnF_2 - and AA-derived photodiodes measured in dark, under a monochromatic light of 940 nm (photon flux $\approx 1.1 \times 10^{13}$) and under 1 sun illumination (100 mW , AM 1.5). Both devices showed clear rectification behavior. However, the AA-derived device possesses a more reduced (over 1 order of magnitude) dark current (i.e., leakage current) under reverse bias compared to that of the SnF_2 -derived device. This lower leakage current can be attributed to the retarded Sn^{2+} oxidation that prevents the generation of associated Sn vacancy for interfacial charge recombination.

For a photodetector, responsivity, i.e., signal-to-noise ratio, is one of the most important parameters to evaluate its efficiency. Generally, the responsivity is strictly linked to the EQE, which represents the ratio of photocurrent to incident light intensity, and can be calculated according to Equation (1)

$$R = \text{EQE} \times \frac{e}{h\nu} \quad (1)$$

where e is the elementary charge, h is the Planck's constant, and ν is the frequency of optical signal. Accordingly, the responsivity of both devices in the NIR region was evaluated and plotted in Figure 3a. For both devices, the corresponding responsivity in the wavelengths between 800 and 950 nm is over 0.2 A W^{-1} , which is comparable to that of the conventional Si-based photodiode.^[27]

Another important FOM for a photodetector is its LDR, which represents a region where the resulting photocurrent has a linear dependency with the incident light intensity. This is important because beyond this range the light signal intensity cannot be precisely detected. The LDR of our fabricated photodiodes was measured by recording the photocurrent under varied light intensities of monochromatic light of 940 nm between $\approx 10^9$ and $\approx 10^{13}$ as shown in Figure 3b.

Intriguingly, the AA-derived photodetector showed a wide LDR extended down to 2×10^9 (photon number) while the LDR of the SnF_2 -derived device deviated from the linear relationship at $\approx 10^{10}$ (photon number). This discrepancy might result from the distinct leakage currents mentioned above. The relatively larger leakage current of the SnF_2 -derived photodiode could ruin the precision of lower intensity light detection compared to the AA-derived device. Note that the EQE of the AA-derived photodiode almost remains constant under varied intensities of monochromatic light (940 nm), which not only affirms its excellent NIR detectivity but also reflects the high quality and stability of the fabricated Sn-containing perovskite device.

The response speed to the incident light of our fabricated device was then examined. Basically, the response speed can be divided into two parts: rising response to light on and decaying process to light off. Those responses are strongly correlated with the thickness of the photoactive layer and charge-transporting interlayers, which dominate the charge transport and collection in device.^[41]

Figure 4a showed the representative photoswitching curves of the AA-derived photodiode to an incident monochromatic light of 940 nm with frequencies of 10 Hz and 50 kHz, respectively. It is worth mentioning that when the switching frequency is small, the resulting photocurrent can show clear “on”

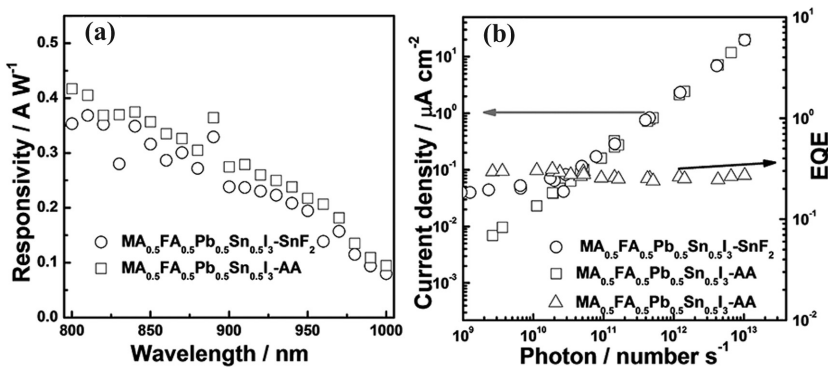


Figure 3. a) Spectral responsivity of the studied photodetectors and b) their corresponding LDR measured under a NIR illumination of 940 nm with varied light intensities.

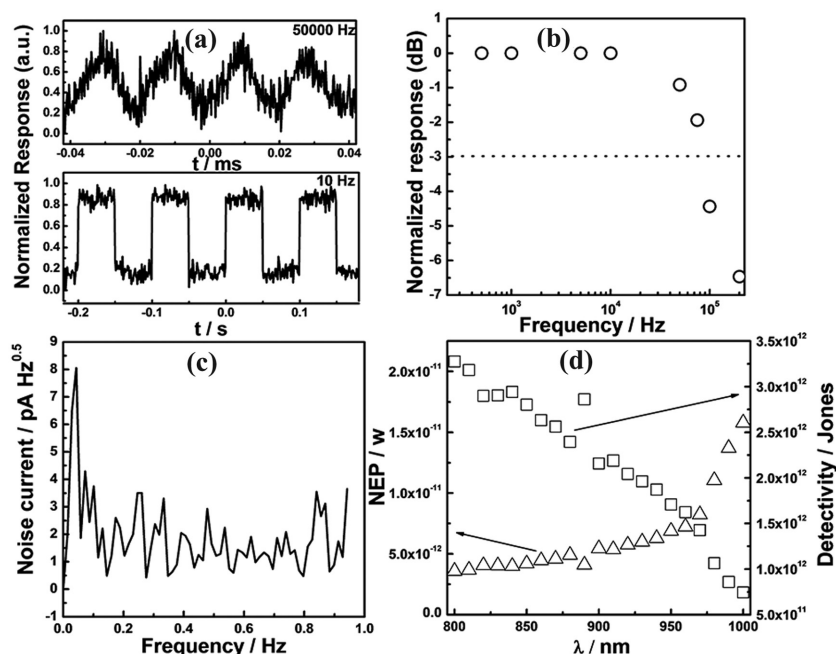


Figure 4. a) Photocurrent response of the AA-derived photodetector (with an active area of 0.8 cm^2) to an optical signal (940 nm) with switching frequencies of 10 Hz and 50 kHz. b) Normalized response loss of the AA-derived photodetectors versus the light modulation frequency at a 940 nm LED. c) Noise current extracted from the Fourier transform of dark current (monitored by Keithley 6430 with Remote PreAmp) of the AA-derived device, and d) its estimated noise equivalent power (NEP) and the detectivity.

and “off” states. However, when the frequency reaches 50 kHz, both rising and decaying processes cannot be fully completed and relaxed. The response of our AA-derived photodiode to the incident monochromatic light (940 nm) with varied switching frequencies is shown in Figure 4b. The resulting photocurrent could only reach $\approx 92\%$ of its maximum value at the steady “on” state when the applied switching frequency was 50 kHz.

The temporal response bandwidth of our photodetector is characterized by a 3 dB bandwidth, which represents a frequency of light signal that yields a photocurrent with a ratio of 0.707 relative to the maximum value obtained at the steady “on” state. For our Sn-containing perovskite NIR photodetector, the -3 dB point frequency ($f_{-3\text{dB}}$) is about 100 kHz, which is almost the same order magnitude as that of MAPbI_3 photodiodes.^[11,13] As mentioned earlier, the response bandwidth is closely correlated with the charge carrier transit time (t) and the resistance–capacitance (RC) time constant, and is limited by the slower between them according to Equation (2)^[40]

$$f_{-3\text{dB}}^{-2} = \left(\frac{3.5}{2\pi t}\right)^2 + \left(\frac{1}{2\pi RC}\right)^2 \quad (2)$$

where R is the total series resistance, including the photodiode resistance, contact resistance, and load resistances in the measurement system; and C is the sum of capacitance of the device and the parasitic capacitance of the measurement system. To assess the limiting factor, the transport time of photogenerated carriers is then investigated since it is germane to t , which can be extracted from the transient photocurrent decay as shown in Figure S5 (Supporting Information). The extracted t of our

AA-derived device is $7.4 \mu\text{s}$. This result suggests that the frequency response of the fabricated NIR photodiode is transit-time-limited. Meanwhile, it also indicates that the selected charge-transporting interlayers in our fabricated photodiode may not be optimal, which is similar to that previously reported.^[42] It warrants more systematic interfacial engineering to further improve the device performance.

The noise of our fabricated NIR photodetector was finally examined, which was characterized from the Fourier transform of its corresponding dark current versus time. As shown in Figure 4c, the estimated noise is $\approx 1.5 \text{ pA Hz}^{-1/2}$ and is frequency independent, which indicates that the white noise dominates the noise current instead of $1/f$ noise. Note that this value was also close to the shot noise limit ($\approx 2.11 \text{ pA Hz}^{-1/2}$) calculated from the dark current using Equation (3)^[12,43]

$$i_s = \sqrt{2qI_d\Delta f} \quad (3)$$

where I_d is the dark current and Δf is the response bandwidth. Here, there are three contributions to the white noise: shot noise, Johnson noise, and thermal fluctuation “flicker,” while the latter two are both related to the thermal agitation.^[44] Taking the testing condition (experiment part) into consideration, it is reasonable to ascribe the shot noise current to dominate noise current, which is also associated with the fluctuations in a measured signal due to the random arrival time of the charge carriers.

Providing the measured noise current and EQE, the NEP and the D^* can be obtained according to the following equations

$$\text{NEP} = \frac{i_n}{R} \quad (4)$$

$$D^* = \frac{\sqrt{A f_{-3\text{dB}}}}{\text{NEP}} \quad (5)$$

where i_n is the noise current, R is the responsivity, and A is the active area. The calculated NEP and D^* of the AA-derived photodiode were plotted in Figure 4d. As can be seen, an excellent detectivity D^* of $>10^{12}$ Jones was achieved for the NIR light between 800 and 970 nm, suggesting the high performance of the fabricated Sn-containing photodetector. Notably, this detectivity for NIR light is comparable to the value achieved for visible light in the MAPbI_3 photodetector.^[11]

3. Conclusion

In summary, we have demonstrated a high-performance NIR photodetector derived from a stable low E_g Sn-containing perovskite, $\text{MA}_{0.5}\text{FA}_{0.5}\text{Pb}_{0.5}\text{Sn}_{0.5}\text{I}_3$. By employing an antioxidant additive, AA, a high-quality $\text{MA}_{0.5}\text{FA}_{0.5}\text{Pb}_{0.5}\text{Sn}_{0.5}\text{I}_3$ film can be

obtained. Moreover, the AA additive can effectively improve the stability of Sn-containing perovskite against oxygen to significantly reduce leakage current. Consequently, the derived photodetector demonstrated high responsivity with a detectivity of over 10^{12} Jones between 800 and 970 nm, rivaling the performance of the conventional inorganic photodetectors. Such a low-cost, solution processable NIR photodetector with high performance demonstrates the great potential of using small-bandgap perovskites for future applications.

4. Experimental Section

General Methods: All chemicals and reagents were purchased from Sigma-Aldrich without further purification. All solutions were filtered with a $0.45\ \mu\text{m}$ PTFE (polytetrafluoroethylene) filter prior to use.

Photodiode Fabrication: ITO glass was first cleaned by detergent followed by ultrasonication with detergent, DI water, acetone, and isopropanol for 10 min immersion, respectively. Then, the substrates were dried by nitrogen flow and treated with ultraviolet–ozone for 20 min before the deposition of PEDOT:PSS. The PEDOT:PSS (AI 4083) solution was spin-coated onto the cleaned ITO glass at 5000 rpm for 30 s and annealed at $150\ ^\circ\text{C}$ for 10 min in air. To prepare the precursor solution of MAPbI₃ perovskite, MAI (159 mg) and PbI₂ (462 mg) were dissolved in a mixed solvent of dimethylformamide (DMF; 630 μL) and dimethylsulfoxide (DMSO; 70 μL) while FAI (172 mg) and SnI₂ (372 mg) were dissolved in a mixed solvent of DMF (800 μL) and DMSO (200 μL) to constitute the precursor solution of FASnI₃.

Finally, the binary metal perovskite precursor solution was prepared by mixing MAPbI₃ (70 μL) and FASnI₃ (100 μL) precursor solutions. Afterward, the 35 μL perovskite precursor was dipped onto the PEDOT:PSS layer and spin-coated at 5000 rpm for 35 s in the glove box. Toluene (700 μL) was dripped in situ onto the substrate at the tenth second. Afterward, the perovskite films were annealed at $100\ ^\circ\text{C}$ for 3 min. PCBM solution (20 mg mL⁻¹ in chlorobenzene) was then spin-coated onto the perovskite film at 2000 rpm for 30 s, followed by the deposition of bis-C₆₀ layer (2 mg mL⁻¹ in isopropyl alcohol, spin-coated at 3000 rpm for 35 s). Finally, Ag electrode with a thickness of 120 nm was evaporated under high vacuum ($<2 \times 10^{-6}$ torr).

Characterization: XRD was measured by an X-ray diffractometer (Bruker F8 Focus Powder for regular XRD and Bruker D8 Discover 2-D XRD for refined XRD). SEM was measured by FEI Sirion and operated at 5 kV. The absorption spectra were measured by a Varian Cary 5000 UV–vis spectrometer. The PL decay measurement was conducted with an IR detector (id 220-FR-MMF, id Quatique SA Geneva/Switzerland). The *J–V* curves were recorded by a Keithley 2400 Source measurement unit; a 450 W xenon lamp was used to produce light; and the light intensity of (100 mW cm⁻²) was calibrated by a standard Si photodiode detector. The EQE spectra were measured by a joint system of a monochromated 450 W xenon lamp (Oriel) and a sourcemeter (Keithley 2400), which calculated using a calibrated Si photodiode (OSI-Optoelectronics).

EIS Measurement: EIS measurements were done using the CHI660E. The Z-view software (v2.8b, Scribner Associates Inc.) was used to analyze the impedance data. The EIS experiments were performed in the dark. The impedance spectra of the MAPbI₃-based devices were recorded at potential of 0 V at frequencies ranging from 0.01 Hz to 1 MHz, the oscillation potential amplitudes being adjusted to 20 mV. The photocathode (ITO attached with NiO) was used as the working electrode, and the Ag counter electrode was used as both the auxiliary electrode and the reference electrode.

Photoswitching Curves: The photoswitching curves of photodiode were measured using a light-emitting diode (940 nm) modulated by the function generator as excitation source. Square waves with different frequency were applied. The photodiode was directly connected to the oscilloscope (Tektronix TDS 684C) with an insert resistor of 50 Ω .

Noise Current Measurement: The noise current was extracted from the dark current which is recorded by a sourcemeter (Keithley 6430 with Remote PreAmp using four-wire sense connections). A Fourier transform was applied.

Supporting Information

Supporting Information is available from the Wiley Online Library or from the author.

Acknowledgements

This work was supported by the Asian Office of Aerospace R&D (FA2386-15-1-4106), the Office of Naval Research (N00014-14-1-0246, N00014-17-1-2260 and N00014-17-1-2201), the National Science Foundation (DMR-1608279), and the Department of Energy SunShot (DE-EE0006710). A.K.-Y. thanks the Boeing-Johnson Foundation for their financial support. The authors also thank Francis Lin for material synthesis, and Liang Gao (Wuhan National Laboratory for Optoelectronics), Prof. Mingkui Wang (Wuhan National Laboratory for Optoelectronics), and Prof. Yang Yang (Zhejiang University) for related discussion.

Conflict of Interest

The authors declare no conflict of interest.

Keywords

low bandgap, near-IR, perovskites, photodetectors

Received: February 25, 2017

Revised: April 5, 2017

Published online: May 16, 2017

- [1] A. Armin, R. Jansen-van Vuuren, N. Kopidakis, P. Burn, P. Meredith, *Nat. Commun.* **2015**, *6*, 6343.
- [2] A. Matsumoto, A. Tamura, R. Koda, K. Fukami, Y. Ogata, N. Nishi, B. Thornton, T. Sakka, *Anal. Chem.* **2015**, *87*, 1655.
- [3] S. Kelley, C. Mirkin, D. Walt, R. Ismagilov, M. Toner, E. Sargent, *Nat. Nanotechnol.* **2014**, *9*, 969.
- [4] L. Zhou, R. Wang, C. Yao, X. Li, C. Wang, X. Zhang, C. Xu, A. Zeng, *Nat. Commun.* **2015**, *6*, 6938.
- [5] L. Li, Y. Huang, J. Peng, Y. Cao, X. Peng, *J. Mater. Chem. C* **2014**, *2*, 1372.
- [6] L. Shen, Y. Zhang, Y. Bai, X. Zheng, Q. Wang, J. Huang, *Nanoscale* **2016**, *8*, 12990.
- [7] L. Shen, Y. Fang, H. Wei, Y. Yuan, J. Huang, *Adv. Mater.* **2016**, *28*, 2043.
- [8] L. Ye, H. Li, Z. Chen, J. Xu, *ACS Photonics* **2016**, *3*, 692.
- [9] L. Ma, W. Hu, Q. Zhang, P. Ren, X. Zhuang, H. Zhou, J. Xu, H. Li, Z. Shan, X. Wang, L. Liao, H. Xu, A. Pan, *Nano Lett.* **2014**, *14*, 694.
- [10] A. Rogalski, J. Antoszewski, L. Faraone, *J. Appl. Phys.* **2009**, *105*, 091101.
- [11] Q. Lin, A. Armin, P. Burn, P. Meredith, *Nat. Photonics* **2015**, *9*, 687.
- [12] Y. Fang, Q. Dong, Y. Shao, Y. Yuan, J. Huang, *Nat. Photonics* **2015**, *9*, 679.
- [13] L. Dou, Y. Yang, J. You, Z. Hong, W.-H. Chang, G. Li, Y. Yang, *Nat. Commun.* **2014**, *5*, 5404.

- [14] X. Xu, Z. Liu, Z. Zuo, M. Zhang, Z. Zhao, Y. Shen, H. Zhou, Q. Chen, Y. Yang, M. Wang, *Nano Lett.* **2015**, *15*, 2402.
- [15] X. Xu, Q. Chen, Z. Hong, H. Zhou, Z. Liu, W.-H. Chang, P. Sun, H. Chen, N. Marco, M. Wang, Y. Yang, *Nano Lett.* **2015**, *15*, 6514.
- [16] S. Stranks, G. Eperon, G. Grancini, C. Menelaou, M. Alcocer, T. Leijtens, L. Herz, A. Petrozza, H. Snaith, *Science* **2013**, *342*, 341.
- [17] G. Xing, N. Mathews, S. Sun, S. Lim, Y. Lam, M. Grätzel, S. Mhaisalkar, T. Sum, *Science* **2013**, *342*, 344.
- [18] A. Kojima, K. Teshima, Y. Shirai, T. Miyasaka, *J. Am. Chem. Soc.* **2009**, *131*, 6050.
- [19] L. Dou, A. Wong, Y. Yu, M. Lai, N. Kornienko, S. Eaton, A. Fu, C. Bischak, J. Ma, T. Ding, N. Ginsberg, L.-W. Wang, A. Alivisatos, P. Yang, *Science* **2015**, *349*, 1518.
- [20] Y. Ogomi, A. Morita, S. Tsukamoto, T. Saitho, N. Fujikawa, Q. Shen, T. Toyoda, K. Yoshino, S. Pandey, T. Ma, S. Hayase, *J. Phys. Chem. Lett.* **2014**, *5*, 1004.
- [21] H. Snaith, *J. Phys. Chem. Lett.* **2013**, *4*, 3623.
- [22] F. Zuo, S. Williams, P. Liang, C. Chueh, C. Liao, A. Jen, *Adv. Mater.* **2014**, *26*, 6454.
- [23] F. Hao, C. Stoumpos, R. Chang, M. Kanatzis, *J. Am. Chem. Soc.* **2014**, *136*, 8094.
- [24] Y. Li, W. Sun, W. Yan, S. Ye, H. Rao, H. Peng, Z. Zhao, Z. Bian, Z. Liu, H. Zhou, C. Huang, *Adv. Energy Mater.* **2016**, *6*, 1601353.
- [25] W. Liao, D. Zhao, Y. Yu, N. Shrestha, K. Ghimire, C. Grice, C. Wang, Y. Xiao, A. Cimaroli, R. Ellingson, N. Podraza, K. Zhu, R. Xiong, Y. Yan, *J. Am. Chem. Soc.* **2016**, *138*, 12360.
- [26] Z. Yang, A. Rajagopal, C. Chueh, S. Jo, B. Liu, T. Zhao, A. Jen, *Adv. Mater.* **2016**, *28*, 8990.
- [27] B. Sutherland, A. Johnston, A. Ip, J. Xu, V. Adinolfi, P. Kanjanaboos, E. Sargent, *ACS Photonics* **2015**, *2*, 1117.
- [28] D. Li, G. Dong, W. Li, L. Wang, *Sci. Rep.* **2015**, *5*, 7902.
- [29] H. Wei, Y. Fang, P. Mulligan, W. Chuirazzi, H.-H. Fang, C. Wang, B. Ecker, Y. Gao, M. Loi, L. Cao, J. Huang, *Nat. Photonics* **2016**, *10*, 333.
- [30] X. Xu, C. Chueh, Z. Yang, A. Rajagopal, J. Xu, S. Jo, A. Jen, *Nano Energy* **2017**, *34*, 392.
- [31] F. Wang, J. Ma, F. Xie, L. Li, J. Chen, J. Fan, N. Zhao, *Adv. Funct. Mater.* **2016**, *26*, 3417.
- [32] Q. Xiong, J. Tu, S. Shi, X. Liu, X. Wang, C. Gu, *J. Power Sources* **2014**, *256*, 153.
- [33] S. Lee, S. Shin, Y. Kim, D. Kim, T. Ahn, J. Noh, J. Seo, S. Seok, *J. Am. Chem. Soc.* **2016**, *138*, 3974.
- [34] M. Kumar, S. Dharrani, W. Leong, P. Boix, R. Prabhakar, T. Baikie, C. Shi, H. Ding, R. Ramesh, M. Asta, M. Graetzel, S. Mhaisalkar, N. Mathews, *Adv. Mater.* **2014**, *26*, 7122.
- [35] Z. Li, H. Chen, H. Bao, M. Gao, *Chem. Mater.* **2004**, *16*, 1391.
- [36] G. Eperon, T. Leijtens, K. Bush, R. Prasanna, T. Green, J. Wang, D. cMeekin, G. Olonakis, V. Milot, R. May, A. Palmstrom, D. Slotcavage, A. Belisle, J. Patel, E. Parrott, R. Sutton, W. Ma, F. Moghadam, B. Conings, A. Babayigit, H.-G. Boyen, S. Bent, F. Giustino, L. Herz, M. Johnston, M. McGehee, H. Snaith, *Science* **2016**, *354*, 861.
- [37] X. Xu, K. Cao, D. Huang, Y. Shen, M. Wang, *J. Phys. Chem. C* **2012**, *116*, 25233.
- [38] A. Guerrero, J. You, C. Aranda, Y. Kang, G. Garcia-Belmonte, H. Zhou, J. Bisquert, Y. Yang, *ACS Nano* **2016**, *10*, 218.
- [39] F. Guo, B. Yang, Y. Yuan, Z. Xiao, Q. Dong, Y. Bi, J. Huang, *Nat. Nanotechnol.* **2012**, *7*, 798.
- [40] M. Casalino, *Int. J. Opt. Appl.* **2012**, *2*, 1.
- [41] L. Shen, Y. Fang, D. Wang, Y. Bai, Y. Deng, M. Wang, Y. Lu, J. Huang, *Adv. Mater.* **2016**, *28*, 10794.
- [42] W. Liao, D. Zhao, Y. Yu, C. Grice, C. Wang, A. Cimaroli, P. Schulz, W. Meng, K. Zhu, R.-G. Xiong, Y. Yan, *Adv. Mater.* **2016**, *28*, 9333.
- [43] G. Konstantatos, I. Howard, A. Fischer, S. Hoogland, J. Clifford, E. Klem, L. Levina, E. Sargent, *Nature* **2006**, *442*, 180.
- [44] X. Gong, M. Tong, Y. Xia, W. Cai, J. Moon, Y. Cao, G. Yu, C. Shieh, B. Nilsson, A. Heeger, *Science* **2009**, *325*, 1665.